International Journal of Heat and Fluid Flow 29 (2008) 1279–1294

Contents lists available at ScienceDirect

International Journal of Heat and Fluid Flow

journal homepage: www.elsevier.com/locate/ijhff

Heat transfer enhancement on a flat surface with axisymmetric detached ribs by normal impingement of circular air jet

Vadiraj Katti, S.V. Prabhu *

Department of Mechanical Engineering, Indian Institute of Technology (I.I.T.), Bombay, Powai, Mumbai 400 076, India

ARTICLE INFO

Article history:
Received 7 February 2008
Received in revised form 8 May 2008
Accepted 19 May 2008
Available online 30 June 2008

Keywords:
Jet impingement
Detached axisymmetric ribs
Heat transfer augmentation

ABSTRACT

An experimental investigation is carried out to study the heat transfer enhancement from a flat surface with axisymmetric detached rib-rougheners due to normal impingement of circular air jet. A single jet from nozzle of length-to-diameter ratio (l/d) of 83 is chosen. Effect of rib width (w), rib height (e), pitch between the ribs (p), location of the first rib from the stagnation point and clearance under the rib (c) on the local heat transfer distribution is studied. Local heat transfer distribution on the impingement surface is investigated for jet-to-plate distances (z/d) varying from 0.5 to 6 using thermal infrared camera. Turbulence intensity using hot-wire anemometer and wall static pressure measurements are reported for the rib configuration in which maximum heat transfer was observed. Contrary to the results of smooth surface, there is a continuous increase in the heat transfer coefficient from the stagnation point in the stagnation region. This trend is well substantiated by the flow distribution in this region. The ratio of average Nusselt numbers of ribbed and smooth surface is seen to increase with Reynolds number. Correlation is developed for Nusselt numbers averaged upto an r/d of 1.5. Enhancements in heat transfer decrease for higher z/d s.

1. Introduction

Impinging jets have received considerable attention due to their inherent characteristics of simple geometry and higher rates of heat transfer. Such impinging flow devices allow for short flow paths on the surface and relatively high rates of cooling from a comparatively small surface area. Various industrial processes involving high heat transfer rates apply impinging jets. Few industrial processes which employ impinging jets are drying of food products, textiles, films and papers; processing of some metals and glass, cooling of gas turbine blades and outer wall of the combustion chamber, cooling of electronic equipments, etc. Heat transfer rates in case of impinging jets are influenced by various parameters like Reynolds number, jet-to-plate spacing, radial distance from stagnation point, Prandtl number, target plate inclination, confinement of the jet, nozzle geometry, curvature of target plate, roughness of the target plate and turbulence intensity at the nozzle exit.

Many prior studies are mostly on jet impinging over flat and smooth surface. Review of the experimental work on heat transfer to impinging jets is reported by Livingood and Hrycak (1970), Martin (1977), Jambunathan et al. (1992) and Viskanta (1993). Gardon and Cobonpue (1962) have reported the heat transfer distribution between circular jet and flat plate for the nozzle plate spacing greater than two times the diameter of jet, both for single jet and array of jets. Specially designed heat flux gages were used for the measurement of local heat transfer distribution from a constant wall temperature plate. Gardon and Akfirat (1965) studied the effect of turbulence on the heat transfer between two-dimensional jet and flat plate. They also studied the heat transfer distribution due to impingement of multiple two-dimensional jets. Gardon and Akfirat (1966), Baughn and Shimizu (1989) and Hrycak (1983) have conducted experiments of heat transfer to round jet from flat plate employing different methods of surface temperature measurement. Lytle and Webb (1994) have studied the effect of very low nozzle-to-plate spacing ($z/d < 1$) on the local heat transfer distribution on a flat plate impinged by a circular air jet issued by long pipe nozzle which allows for fully developed flow at the nozzle exit. They observed that for lower nozzle-to-plate spacing ($z/d < 0.25$), maximum Nusselt number shifts from the stagnation point to the point of secondary peak and is more pronounced at higher Reynolds number. Lee et al. (2004) have studied the influence of nozzle diameter on impinging jet heat transfer and fluid flow. They reported that local Nusselt numbers in the region of $0 \leqslant r/d \leqslant 0.5$ increase with larger nozzle diameters. Katti and Prabhu (2008) reported experimental investigations and analysis of local heat transfer distribution on a flat surface due to jet impingement from a long pipe nozzle. Three regions are identified on the target surface namely stagnation region, transition region and wall jet region based on heat transfer distribution. Semi-empirical correlations for local Nusselt numbers separately for each region are reported.

* Corresponding author. Tel.: +91 22 25767515; fax: +91 22 2572 6875/3480.
E-mail addresses: svprabhu@iitb.ac.in, svprabhu@me.iitb.ac.in (S.V. Prabhu).

0142-727X/$ - see front matter © 2008 Elsevier Inc. All rights reserved.
doi:10.1016/j.ijheatfluidflow.2008.05.003

Nomenclature

A	surface area for smooth surface (m^2)
c	clearance under the rib (m)
d	diameter of the nozzle at exit (m)
e	height of the rib (m)
h	heat transfer coefficient (W/m^2 K)
I	current (A)
k	thermal conductivity of air (W/m K)
l	length of the nozzle pipe (m)
Nu	Nusselt number (hd/k)
$\overline{Nu}_r$	average Nusselt number over ribbed surface
$\overline{Nu}_s$	average Nusselt number over smooth surface
p	pitch between the ribs (m)
ΔP	differential wall static pressure (Pa)
q	heat flux (W/m^2)
q_{con}	net heat flux convected to the impinging jet (W/m^2)
q_{joule}	imposed Ohmic heat flux, (VI/A) (W/m^2)
q_{loss}	total heat flux lost from impingement plate (W/m^2)
$q_{rad(f)}$	radiation loss from the front surface of impingement plate (W/m^2)
$q_{rad(b)}$	radiation loss from the back surface of impingement plate (W/m^2)
q_{nat}	heat loss due to natural convection from the back surface of impingement plate (W/m^2)
r	radial distance from the stagnation point (m)
r_1	radial location of first rib (m)
Re	Reynolds number, ($\rho\overline{V}d/\mu$)
T_j	jet air temperature (K)
T_r	temperature of the target plate at given radial location (K)
u'	near-wall turbulent intensity (m/s)
U_r	near-wall radial velocity (m/s)
V	voltage (V)
$\overline{V}$	average velocity of flow at nozzle exit (m/s)
w	width of the rib (m)
y	normal distance from the surface of target plate(m)
z	nozzle plate spacing (m)

Greek symbols

μ	viscosity of air (Pa s)
ρ	density of air corresponding to supply pressure (kg/m^3)

The influence of surface rougheners on heat transfer enhancements are reported in literature. Hansen and Webb (1993) have studied the effect of the modified surface on the average heat transfer between impinging circular jet and the flat plate. They have found that for the pyramidal, short square and intermediate square fins, there is an increase in the average Nusselt number value by 12–23% and reduction in the value of the average Nusselt number by 4–38% for the other types of fins studied. The effect of surface rougheners, in the form of cubes, on the heat transfer between impinging jets and flat plate are studied in Chakroun et al. (1998). They have reported the heat transfer augmentation up to 8–28%. However, their data reflects the average Nusselt number variation rather than local data because of the large thickness of the target plate (brass plate of 10 mm thick) used. Ekkad and Kontrovitz (2002) have studied the effect of the dimpled surface on the heat transfer between array of circular jets and the flat plate. They have reported reduction in the heat transfer coefficient for the dimpled surface as compared to the smooth surface.

Miyake et al. (1994) studied heat transfer characteristics of an axisymmetric jet impinging on a wall with eleven concentric attached square ribs as roughness elements ($0 < r/d < 5.0$). Each rib is machined on concentric copper target surface (10 mm thick) are separated and heated individually so as to form isothermal surface. Thus, radial distribution of annular segment averaged heat transfer coefficients is presented. Only two concentric rib segments are located in the stagnation region and hence heat transfer distribution reported for this region may not be truly local. Nusselt numbers at each rib location are reported higher than the corresponding smooth surface. The ribbed surface with $p/e = 5.0$ and $e/d = 0.1$ is reported to have higher heat transfer augmentation. At lower z/d (3.0), Nusselt numbers in the stagnation region are lower than the corresponding case of smooth surface and they attributed it to the formation of a dam in the stagnation region by the first axisymmetric rib. In the downstream, Nusselt number increase by about 30% at an $r/d = 1.0$ and further decay monotonically. Fourth order polynomial curve fit correlations for radial Nusselt number distribution are reported for each configuration. Gau and Lee (1992, 2000) have reported the heat transfer augmentation to slot jet impinging on square ribbed and triangular ribbed walls, respectively. Constant heat flux heater surface is used in their experiments. Thermally active attached ribs on such a surface will have lower base temperatures and its effect is felt on adjacent area of rib base. Hence, it may be observed that heat transfer coefficients estimated from surface temperature distribution show higher values under the rib and its adjacent locations where there is no flow. Thus, the augmentations reported may be due to combined effect of two factors, namely (a) the enhanced turbulence mixing by distorting the flow fields caused by the presence of ribs and (b) the extension in heat transfer surfaces i.e., the fin effect caused by the ribs.

Few studies are reported on the heat transfer characteristics due to detached ribs in the internal flow situation. Tsia and Hwang (1999) have studied the effect of thermal conductivity of the attached ribs in internal flow using thermally active material (aluminum ribs) and thermally non-active turbulators (wood ribs). They concluded that higher enhancements with thermally active ribs are attributed to rib conduction effects. Their experiments with fully detached ribs show enhanced heat transfer due to enhanced turbulence. They speculated the flow over the detached ribs and reported shedding of vortices from the detached rib and the wall jets ejecting from the rib clearance. Liou and Wang (1995) and Liou et al. (1995) have studied different configurations of detached ribs on the walls in internal flows and reported improved thermal performance compared to the attached ribs. They reported higher forced convection resulting from higher acceleration of the flow between the rib base and the heated wall. The flow visualization results of Liou et al. (1998) show the presence of recirculating flow immediately behind the detached rib. They also observed an asymmetric wake behind the rib because of asymmetric flow area across the rib. The vortex shedding promotes the mixing of fluid and hence leads to a higher level of heat transfer distributions. Liou et al. (1997) have made LDV measurements for flows over detached ribs. They showed that the wake generates higher convective velocity and turbulent kinetic energy in the region behind the rib. This provides better heat transfer augmentation immediately behind the rib and depends on the clearance under the rib.

There is no information available on the heat transfer distribution on the flat plate with detached axisymmetric ribs due to jet

impingement. Hence, the objective of the present study is to experimentally investigate the role of detached ribs on the heat transfer augmentation of a flat surface impinged by a normal jet. The influence of rib width, rib height, pitch between the ribs, location of the first rib from the stagnation point and clearance under the rib on the local heat transfer distribution is to be studied sequentially to arrive at a better configuration.

2. Experimental apparatus and procedure

The experimental set-up layout is shown in Fig. 1. Laboratory air compressor supplies air to the nozzle through a calibrated orifice flow meter. Air filter and pressure regulator are installed upstream of the orifice flow meter to filter the air and to maintain the downstream pressure at a value of 4 bar. The flow rate is controlled by two needle valves, one on each side of the orifice flow meter. The function of the upstream needle valve is not to allow cooling air to flow until the compressor has built up the pressure in its reservoir above 4 bar. Actual flow rate is controlled by the downstream needle valve. The nozzle is constructed with an acrylic pipe of inner diameter of 15 mm and length to diameter ratio of 83. This length is sufficient to ensure fully developed flow over the Reynolds number range investigated. The end of the nozzle is machined perpendicular to the nozzle axis.

The target plate assembly for heat transfer distribution is shown schematically in Fig. 2a. The heater which also acts as a target plate (80 mm × 160 mm; 0.06 mm thick) made of stainless steel foil is firmly clamped and stretched between the two copper bus bars. Approximately 5 mm of the foil on either side is sandwiched in the bus bars to ensure proper grip. Because of the thinness of foil,

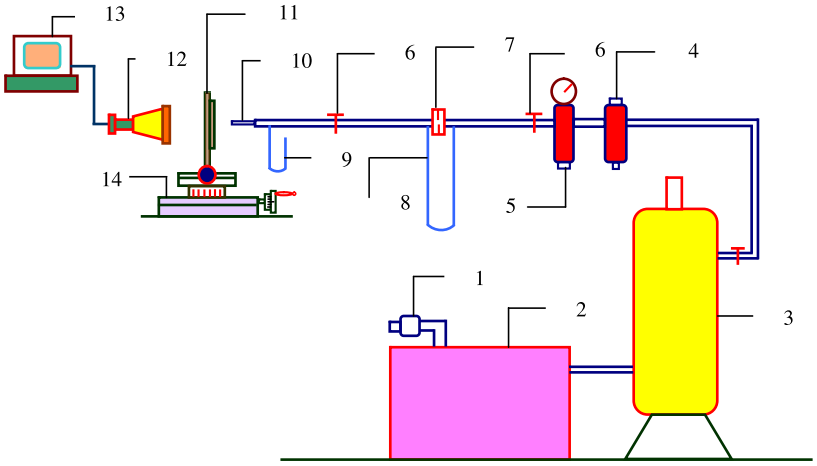

1) Air filter. 2) Air compressor. 3) Air receiver. 4) Air filter. 5) Pressure regulator.
6) Needle valves. 7) Orifice plate. 8) Differential manometer. 9) Simple manometer.
10) Nozzle.11) Impingement plate assembly. 12) Infra red camera. 13) Computer.
14) Compound slide with swivel base.

Fig. 1. Layout of Experimental set-up.

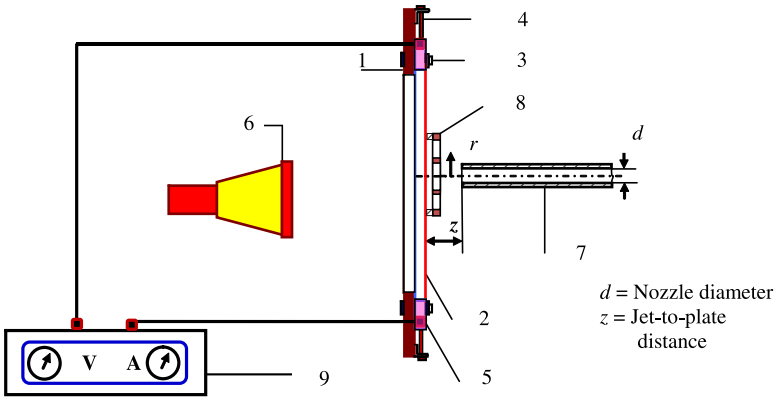

1). Frame. 2) Stainless steel foil. 3) Clamping screw 4) Stretching screw. 5) Copper bus bar.
6) I.R.Camera.7) Long-tube nozzle 8) Detached rib assembly
9) Regulated DC power supply

Fig. 2a. Target plate assembly for heat transfer distribution.

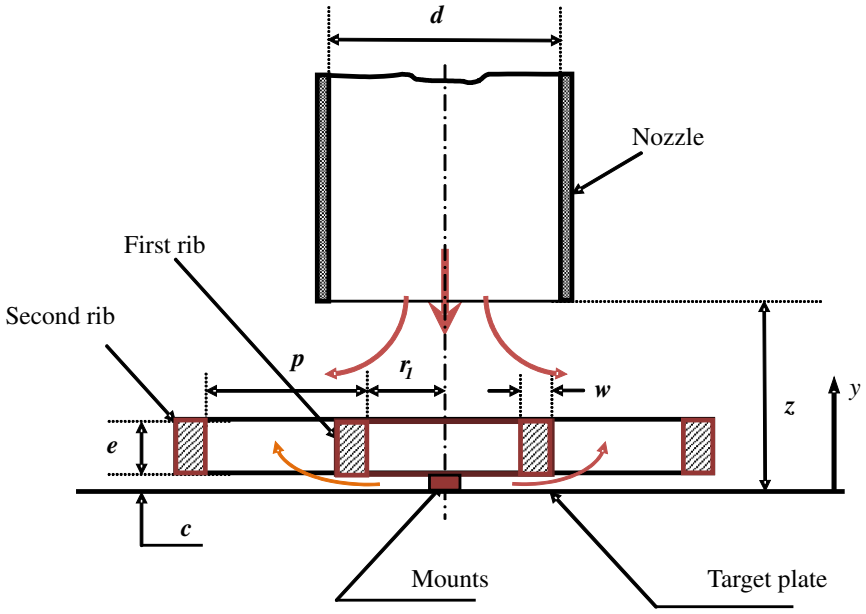

d = Nozzle diameter; z = Jet-to-plate distance; c = Clearance under the rib;
e = Height of the rib; w = Width of the rib; r_1 = Radius of the first rib;
p = Radial distance between the ribs (Pitch)

Fig. 2b. Geometry of axisymmetric detached rib with jet impingement.

lateral conduction is negligible and surface provides constant heat flux situation as reported by Lytle and Webb (1994). Thermal images are obtained from *IR* camera positioned on the side of the heater opposite the impinging nozzle. One-dimensional energy balance across the heated plate shows negligible temperature difference across it. Hence, the local temperature measured on the back surface is considered to be same as that on the impingement plane. The back surface of heater element is painted black using a thin coat of 'Matte finish Asian' paint which provides high emissivity (0.99) surface. Infrared radiometry technique provides higher spatial resolution of temperature than thermocouples. 'Thermoteknix' Ti200 infrared camera used during present experimentation allows for a spatial resolution of about 0.4 mm per pixel.

The geometry of the axisymmetric detached rib on target plate and coordinates are shown in Fig. 2b. The axisymmetric ribs are fabricated from thermally non-active material (plexiglass, $k = 0.23$ W/mK) as rings of rectangular cross section and pasted on the surface with two mounts at diametrically opposite locations. The height of each mount is equal to the clearance under the ribs to detach it from the target surface. Power is supplied from a regulated *DC* power supply. Proper voltage taps are provided in each of the bus bars. The voltage across the heater is measured by digital voltmeter whose range and the accuracy is of 0–20 V ± 0.5%. The current through the heater is measured from the digital indicator on the panel of *DC* power supply. Jet air temperature is measured using a Chromel–Alumel thermocouple (K-type) positioned at the nozzle inlet. The output of the thermocouple is measured using a digital millivoltmeter. Two-axis traverse system

Table 1
The range of values of the parameters studied

Sl. no.	Parameters	Range of values studied
1	Clearance under the ribs (c/d)	0.033, 0.067, 0.1 and 0.133
2	Width of the rib (w/d)	0.23 and 0.13
3	Height of the rib (e/d)	0.13, 0.23, 0.33 and 0.4
4	Location of the first rib (r_1/d)	0.33, 0.4 and 0.5
5	Pitch between the ribs (p/e)	2.0, 4.0 and ∞ (single rib)
6	Reynolds number (Re)	5000, 10000, 15000 and 20000
7	Jet-to-plate spacing (z/d)	0.5, 1.0, 2.0, 3.0, 4.0 and 6.0

Table 2
Uncertainties of the parameters

Parameter	% Uncertainty at	
	Re = 5000	Re = 20000
Reynolds number	1.6	1.5
Nusselt number	4.8	3.8
Wall static pressure	0.5	0.5
Near-wall turbulent intensity	3.0	
Near-wall radial velocity	3.0	

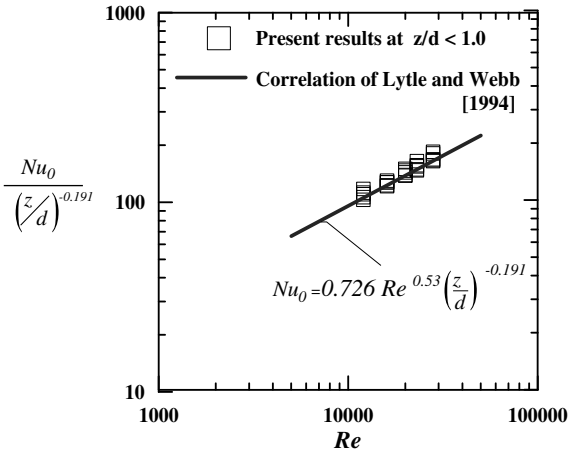

Fig. 3. Comparison of present results with the correlation of Lytle and Webb (1994).

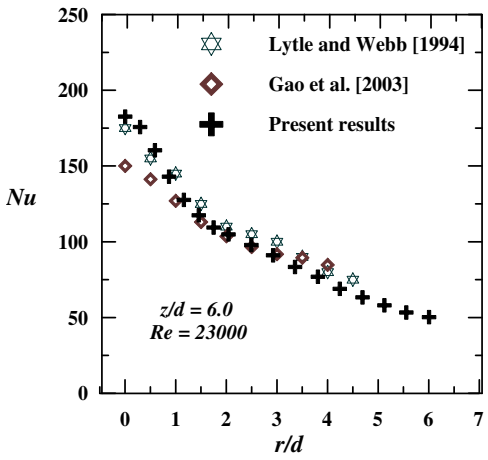

Fig. 4. Comparison of the present results with those of previous researchers for radial distribution of Nusselt number.

is used to position the target plate and set different jet-to-plate distances.

Thermal infrared camera reads the temperature of the plate depending on the emissivity value of the surface of the plate. Therefore, it is necessary to calibrate the emissivity of the surface. Detailed procedure is reported in Katti and Prabhu (2008). The average emissivity is found to be 0.99. The uncertainty in the temperature measurement is not more than ±0.5 °C. Power loss from the exposed surface of the target plate due to natural convection and radiation is estimated experimentally. The corrections are included in the calculation of local heat transfer coefficient.

Radial distribution of near-wall turbulent intensity and velocity is measured using Hot-Wire Anemometry. The system is a TSI model IFA 300 Constant Temperature Anemometer System with TSI probe 1210-10 number 70618124. The probe is traversed in the radial direction with tip located at 1 mm from the target surface. Local wall pressure measurements are made on the same set-up by replacing the stainless steel heater foil with an acrylic plate. Small holes of approximately 0.5 mm in diameter are drilled in the plate of 10 mm thick for 3 mm deep from impingement surface and then counterbored to 3 mm diameter for the remaining depth. These holes from the back are connected to U-tube manometer via tubing which measures wall static pressures. The nozzle is aligned normal to and inline with central hole and the table is traversed parallel to the nozzle axis for different jet-to-plate spacing.

Various parameters which influence the distribution of heat transfer coefficients on flat target surface with axisymmetric detached ribs are as follows:

- Clearance under the rib, c/e
- Height of the rib, e/d
- Width of the rib, w/d
- Location of the first rib, r_1/d
- Pitch between the ribs, p/e
- Jet-to-plate distance, z/d

The range of values of the various parameters considered in the present study is listed in Table 1.

3. Data reduction

The temperature distribution on the target plate is obtained by averaging ten thermal images for each configuration. Digitization of thermal images for temperature distribution on impingement surface is carried out in MATLAB. The Nusselt number for the smooth and ribbed surface is calculated by

$$Nu = \frac{hd}{k} \tag{1}$$

$$h = \frac{q_{\text{conv}}}{T_{\text{r}} - T_{\text{j}}} \tag{2}$$

$$q_{\text{conv}} = q_{\text{joule}} - q_{\text{loss}} \tag{3}$$

$$q_{\text{loss}} = q_{\text{rad}(f)} + q_{\text{rad}(b)} + q_{\text{nat}} \tag{4}$$

$$q_{\text{joule}} = \frac{VI}{A} \tag{5}$$

$$q_{\text{loss}} = q_{\text{rad}(f)} + q_{\text{rad}(b)} + q_{\text{nat}}. \tag{6}$$

(Estimated experimentally)

Table 3
Parametric study of detached ribs at a constant Reynolds number of 20,000

Sl. no.	Rib parameters varied	Rib parameters fixed	Jet-to-plate spacing	Conclusion
1	*Clearance under the rib* c/d = 0.03, 0.067, 0.1, and 0.133	e/d = 0.23 w/d = 0.23 Number of ribs = 2 First rib at r_1/d = 0.5 p/e = 4.0	z/d = 0.5, 1.0, 2.0, 3.0, 4.0, 6.0	Rib clearance c/d = 0.067 is a better configuration
2	*First rib location* r_1/d = 0.5, 0.4 and 0.33	e/d = 0.23 w/d = 0.23 c/d = 0.067 Number of ribs = 2 First rib at r_1/d = 0.5 p/e = 4.0	z/d = 0.5, 1.0, 2.0, 3.0, 4.0, 6.0	First rib located at r_1/d = 0.33 is a better configuration
3	*Rib width* w/d = 0.23 and 0.13	e/d = 0.23 c/d = 0.067 Number of ribs = 2 First rib at r_1/d = 0.33 p/e = 4.0	z/d = 0.5, 1.0, 2.0, 3.0, 4.0, 6.0	w/d = 0.13 performs better
4	*Pitch* p/e = 2, 4 and ∞ ($p/e = \infty$, single rib)	e/d = 0.23 w/d = 0.13 c/d = 0.067 Number of ribs = 2 First rib at r_1/d = 0.33	z/d = 0.5, 1.0, 2.0, 3.0, 4.0, 6.0	Better with single rib ($p/e = \infty$) at an r_1/d = 0.33
5	*Height of the rib* e/d = 0.13, 0.23, 0.33 and 0.4	w/d = 0.13 c/d = 0.067 Single rib at r_1/d = 0.33 i.e., $p/e = \infty$	z/d = 0.5, 1.0, 2.0, 3.0, 4.0, 6.0	e/d = 0.23 performs better for all z/ds except z/d = 0.5

Contour maps for Nusselt number distribution on the target surface with and without ribs are obtained from MATLAB. Uncertainties in the estimation of different parameters are carried out using the method suggested by Moffat (1988) and are listed in the Table 2.

4. Results and discussion

In the present study, first the baseline experiments are carried out with the jet impinging normally on a smooth surface. To validate the experimental technique and procedure, Nusselt number distribution is compared with that of Lytle and Webb (1994). Fig. 3 shows stagnation point Nusselt numbers from the present study and are in good agreement (within 4.8%) with the correlations for low z/d (less than 1.0) of Lytle and Webb (1994). The local Nusselt number at a Reynolds number of 23,000 and z/d of 6 is compared with those of the earlier published data as shown in Fig. 4. It compares well with the results of Lytle and Webb (1994) and Gao et al. (2003).

4.1. Heat transfer studies

Sequential parametric study is conducted in an effort to obtain a configuration of better heat transfer characteristics on the target plate. The influence of each parameter is studied for nozzle-to-

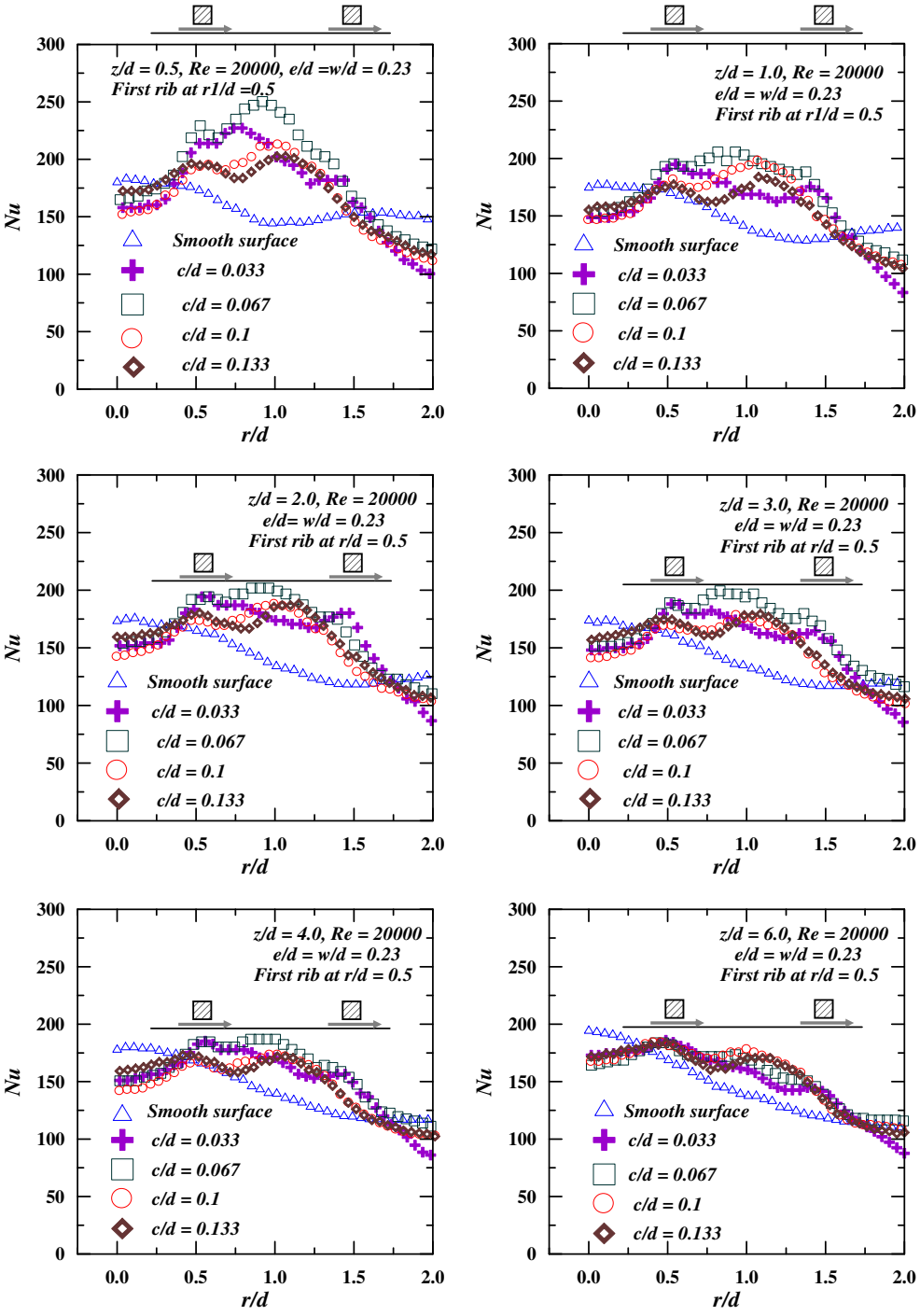

Fig. 5. Effect of rib clearance on radial distribution of heat transfer to impinging axisymmetric jet from surface of detached ribs (two ribs, $p/e = 4.0$).

plate distance varied from 0.5 d to 6 d and at a Reynolds number of 20,000. The discussion is presented in the following paragraphs and summarized in Table 3.

4.1.1. Effect of the rib clearance

Effect of the rib clearance on the radial heat transfer distribution is studied for four clearance heights i.e., $c/d = 0.033$, 0.067, 0.1 and 0.133. Rib height ($e/d = 0.23$), rib width ($w/d = 0.23$), two ribs with pitch ($p/e = 4$) and location of the inner rib at $r_1/d = 0.5$ are kept constant. Fig. 5 represents the local distribution of Nusselt number for different clearance heights and is compared with a corresponding case of jet impingement on smooth surface. Heat transfer rate at the stagnation point is lower for all the ribbed cases by around 10–15% than the smooth surface case. These differences are more pronounced for z/d s other than 0.5. It is observed that, in general, Nusselt number increases towards the first rib and reaches maximum at $r/d = 0.5$ which corresponds to inner radial location of first rib. This may be attributed to acceleration of fluid in that region created by clearance under the rib. However, for $c/d = 0.1$ and 0.067 reach the same value of maximum Nusselt numbers

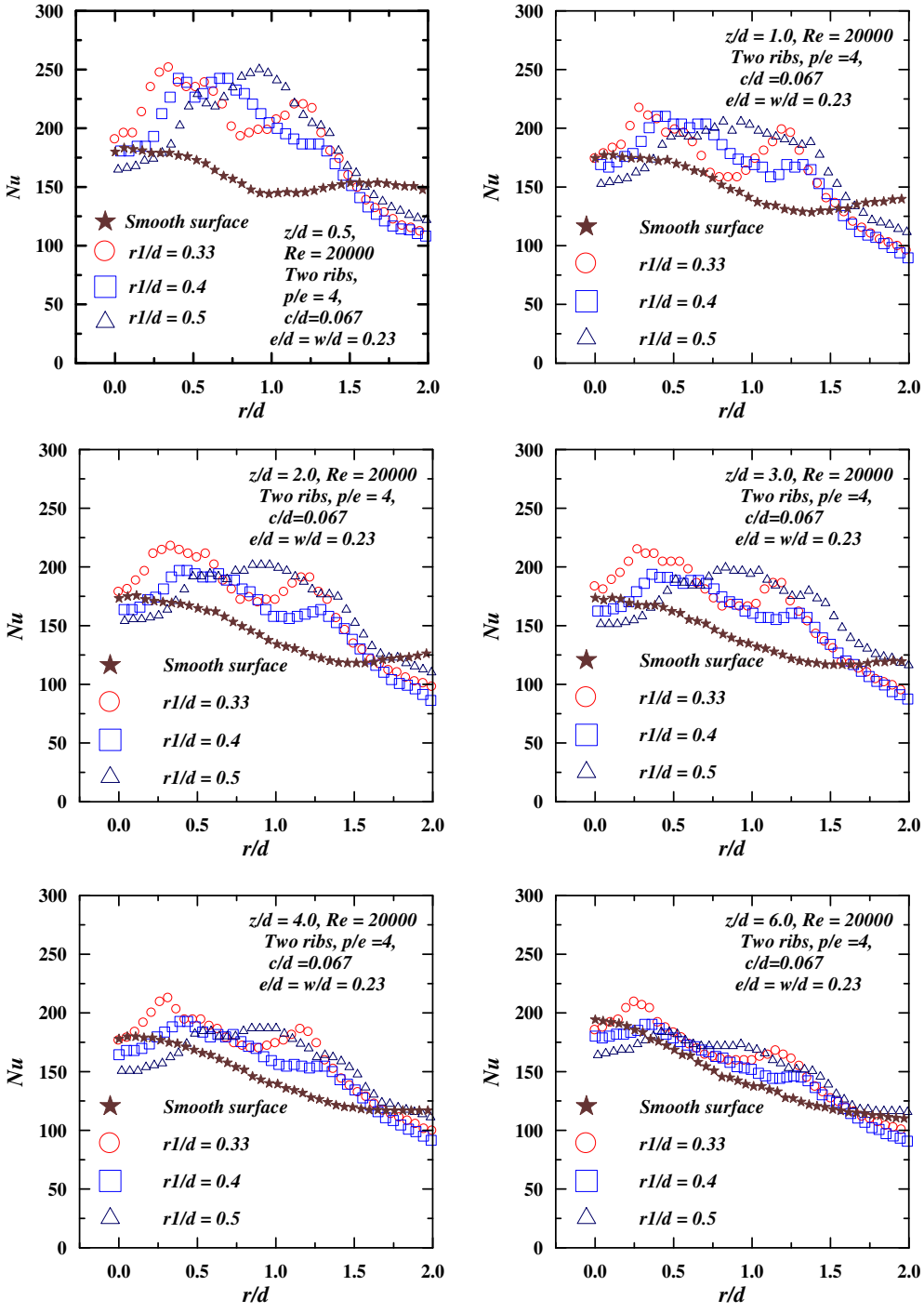

Fig. 6. Effect of location of inner rib on radial heat transfer distribution to impinging air jet on surface of detached ribs.

but for $c/d = 0.033$ and 0.133 the values are lower for all z/d s except for 6.0. Under the first rib, the Nusselt numbers are fairly constant for all clearances and for all z/d s. Downstream of the first rib, Nusselt number drops to a minimum and then forms a peak. The drop in the values of Nusselt number is higher for higher clearances. It is observed that the heat transfer coefficients peak at different radial locations for different clearances. For $c/d = 0.033$, 0.067, 0.1 and 0.133 the peaks occur, respectively, at r/d approximately equal to 0.8, 0.9, 1.0 and 1.1. This peak and their location may be attributed to combined effect of reattachment of flow over the rib and transition of radial wall jet exiting under the rib. For larger detachment distances of ribs increases the overall height of the rib and thus flow reattachment may occur at larger radial distances. Moreover, with increase in the clearance heights under the rib, transition may occur at larger radial distances downstream of the first rib.

The flow crosses the second rib at $r/d = 1.43$ corresponding to $p/e = 4$. Heat transfer coefficients slightly increase just ahead of the second rib and this may be again due to acceleration effects, significantly observed for $c/d = 0.033$ and 0.067. For higher clearances,

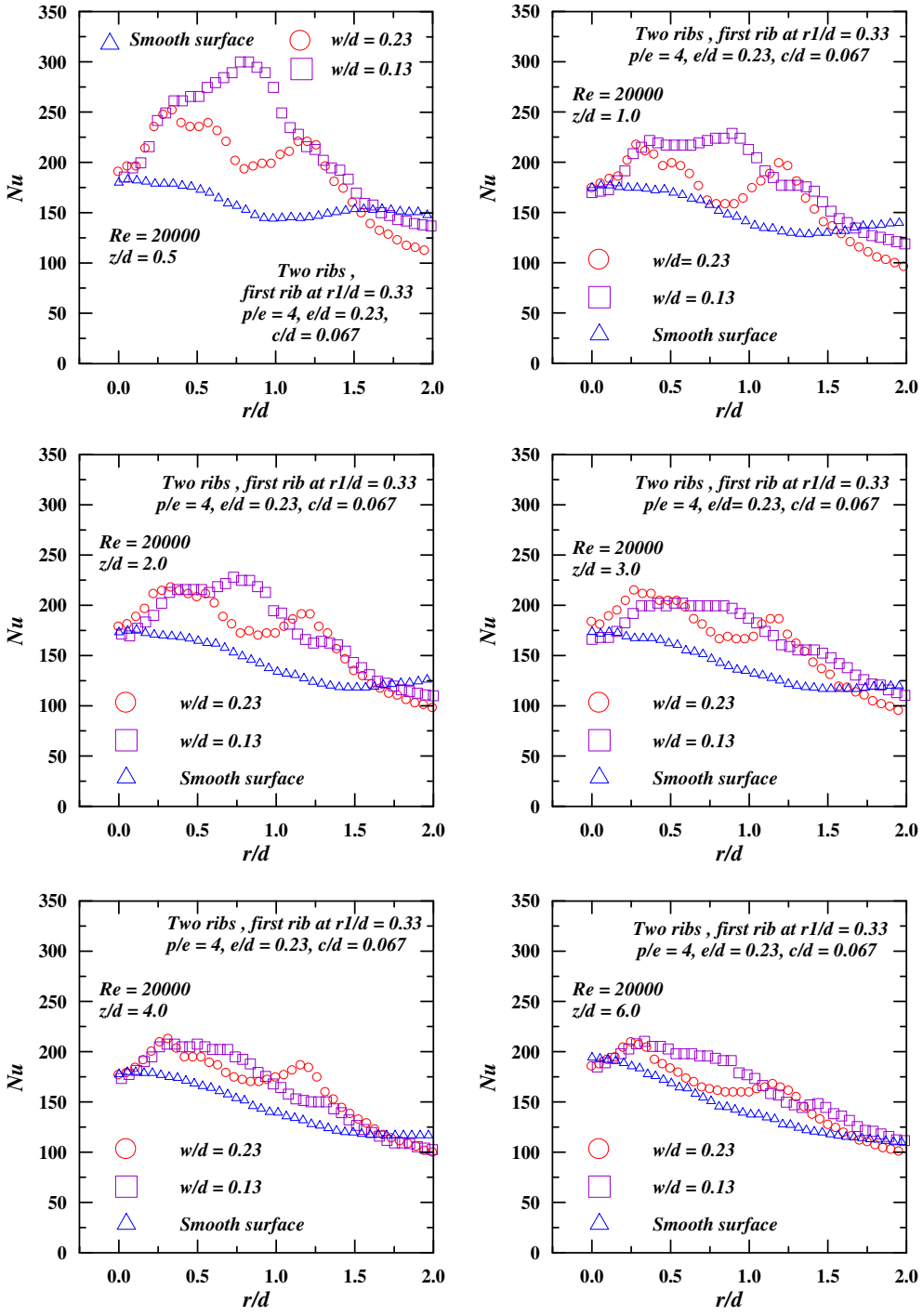

Fig. 7. Effect of rib width on local heat transfer distribution to impinging circular jet on flat surface with detached ribs.

second rib does not show any influence on heat transfer distributions. Downstream of the second rib heat transfer coefficients attenuate monotonically for all rib clearances and the decay rate is higher for lower clearances. Average Nusselt numbers upto $r/d = 2.0$ are higher for c/d of 0.067 compared to all other clearances studied.

4.1.2. Effect of the inner rib location (r_1/d)

The best case from the previous configuration, a rib clearance of $c/d = 0.067$ is chosen to study the influence of radial location of the first rib from stagnation point. Other parameters like rib height ($e/d = 0.23$), rib width ($w/d = 0.23$) and two ribs with pitch ($p/e = 4.0$) are kept constant. Different inner rib locations studied are $r_1/d = 0.33$, 0.4 and 0.5. Fig. 6 shows the radial distribution of Nusselt number for this configuration at $z/d = 0.5$, 1.0, 2.0, 3.0, 4.0 and 6.0. It is seen that the effects observed under the first rib during study of previous configuration also exist in this case. However, the Nusselt numbers at the stagnation point increase with decrease in r_1/d for all z/d s. For $r_1/d = 0.33$, Nusselt number at the stagnation point are nearly equal to or slightly higher than a case of impingement on smooth surface. This may be due to fluid acceleration effects because of detachment of ribs extending towards the stagnation with

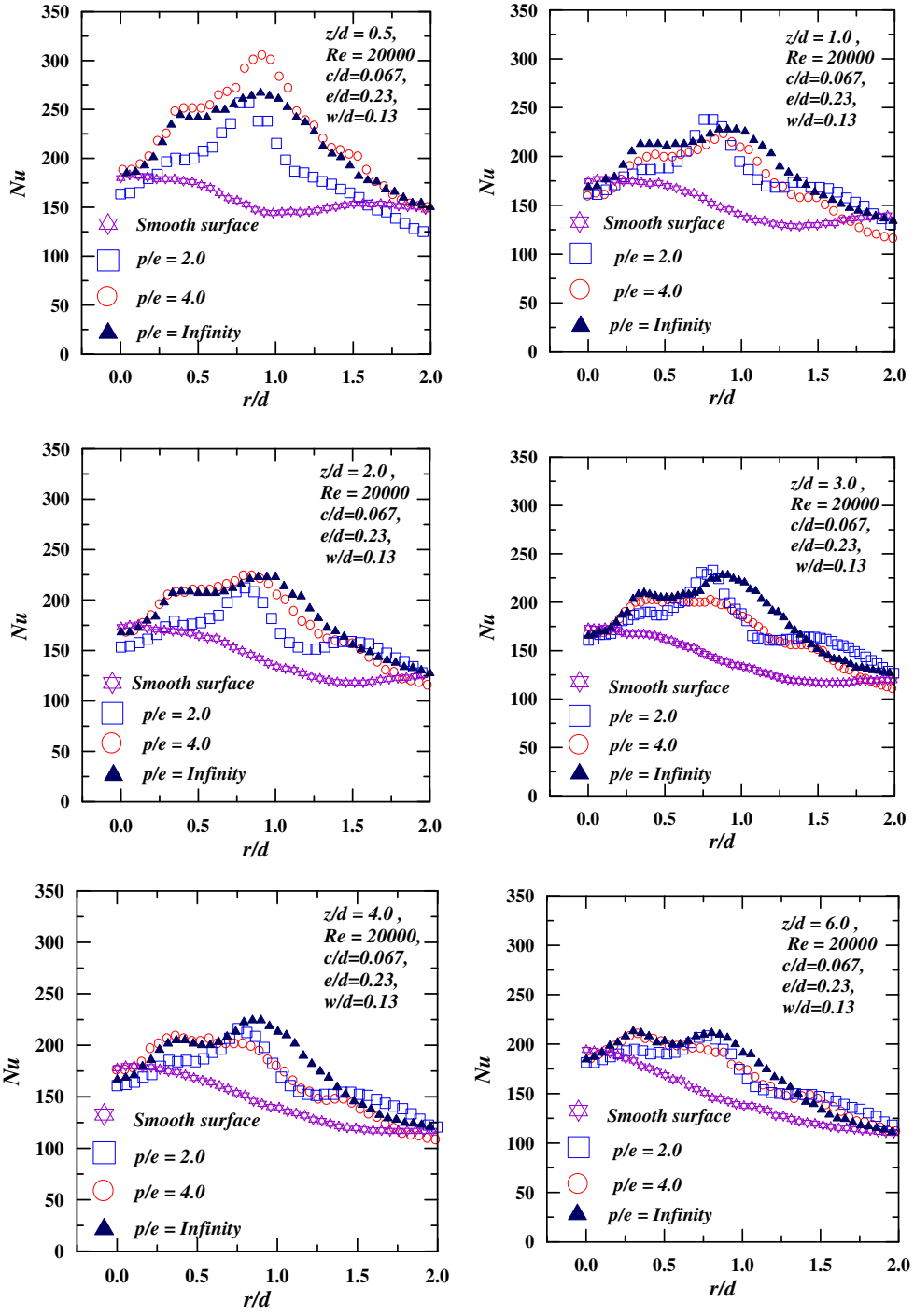

Fig. 8. Effect of pitch between ribs on local distribution of Nusselt number to impinging jet on surface with detached ribs.

shifting of first rib nearer the stagnation. Downstream of the first rib, Nusselt number drops to a minimum and then forms a peak, similar to the observation in the previous case. But, for the inner rib located at $r_1/d = 0.33$ and 0.4, the existence of the second rib is not significantly felt. Region near stagnation point up to an r/d of about 0.5, heat transfer coefficients for the inner rib located at $r_1/d = 0.33$ are higher for all z/d s.

4.1.3. Effect of the rib width (w/d)

The clearance under the ribs of $c/d = 0.067$ and inner rib location at $r_1/d = 0.33$ is considered as the better combination among the configurations studied. The influence of the rib width is investigated keeping height of the rib ($e/d = 0.23$) and two ribs with pitch ($p/e = 4.0$) constant. Fig. 7 shows the effect of the rib width on the radial distribution of heat transfer coefficients upto an $r/d = 2.0$. Nusselt numbers at the stagnation point does not significantly vary with different rib widths and no rib at a given z/d. The effects under the first rib are same as depicted in earlier cases. However, in the downstream of the first rib, some contrasting effects are observed. For rib width of $w/d = 0.23$, major jet flow at its periphery impinges on the top surface of the rib and may not reach the target surface. In turn, the target surface does not get exposed directly to this part

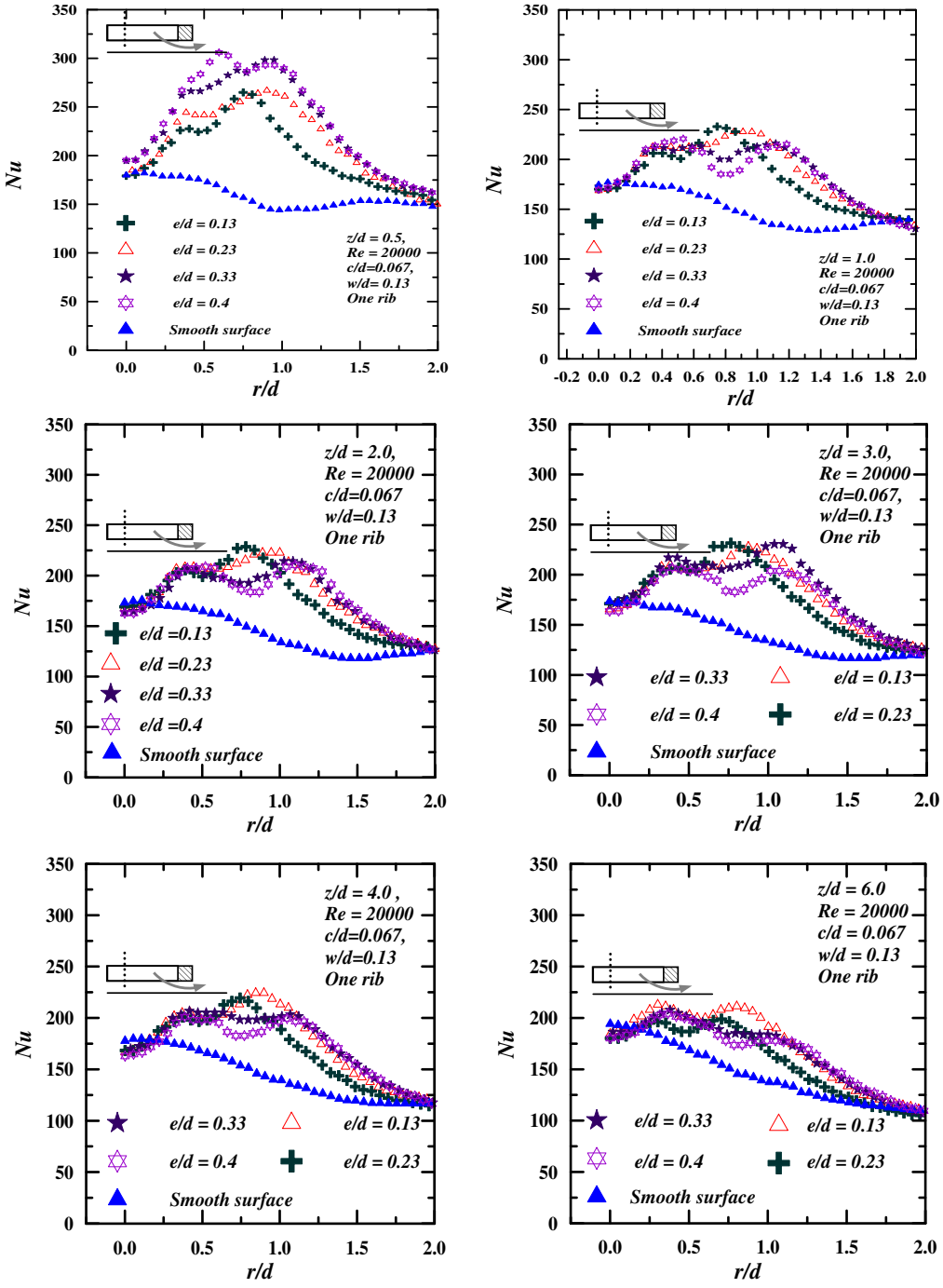

Fig. 9. Effect of rib height on radial distribution of Nusselt number to impinging circular jet on flat surface with detached ribs.

of impinging flow. Hence, heat transfer coefficients are seen to decrease in this region. But for the rib width of $w/d = 0.13$, jet flow impinging on rib top reduces considerably. Hence decrease in the heat transfer coefficients observed with rib width of $w/d = 0.23$ in this region vanish. However, heat transfer rates increase again just ahead of the second rib. Heat transfer coefficient distribution is observed to be fairly uniform from the first rib till an r/d of about 1.0 and for z/d greater than 1.0. Thus it can be concluded that rib width (w/d) of 0.13 has better heat transfer characteristics than rib width (w/d) of 0.23.

4.1.4. Effect of the pitch between ribs (p/e)

The influence of pitch between the ribs on heat transfer distributions is studied for two ribs with $p/e = 2.0$, 4.0 and ∞ (no second rib). From the previous parametric study, the rib clearance (c/d) = 0.067, inner rib located at $r_1/d = 0.33$ and rib width (w/d) = 0.13 are the rib parameters chosen as they provide better heat transfer characteristics. The rib height $e/d = 0.23$ is considered in this study. Fig. 8 shows radial heat transfer distributions for different p/e ratios. The stagnation point Nusselt numbers of detached ribs for the given z/d is nearly same and comparable with that of smooth surface. The heat transfer coefficients under the first rib are slightly lower for $p/e = 2.0$. This may be due to reduction in the flow accelerations under first rib in the presence of closer second rib. Radial location of peak after the first rib occurs just ahead of second rib. But, local Nusselt numbers between this peak and the first rib for $p/e = 2.0$ are lower than the cases of $p/e = 4.0$ and ∞. Except for $z/d = 0.5$, it is observed that average heat transfer coefficients up to $r/d = 1.25$ is higher for case of only single rib ($p/e = \infty$).

4.1.5. Effect of rib height (e/d)

All previous parametric studies show that a single rib at $r_1/d = 0.33$, clearance under the rib (c/d) of 0.067 and width of the rib (w/d) of 0.13 is a better configuration. The effect of height of the ribs on the local heat transfer distribution to impinging circular jet is studied keeping these values of parameters stated above. Heights chosen for investigation are $e/d = 0.13$, 0.23, 0.33 and 0.4. Fig. 9 shows the influence of rib height on the radial heat transfer distributions. Nusselt number distribution patterns are similar for all the z/d s except for a z/d of 0.5. For z/d s other than 0.5, stagnation Nusselt numbers are same as that of the case of smooth surface. Heat transfer distributions up to the first rib remain almost identical for all z/d except 0.5 and 6.0. The locations of peak occur at different radial locations. The higher the rib height farther is this location from stagnation point. However, the locations of peaks

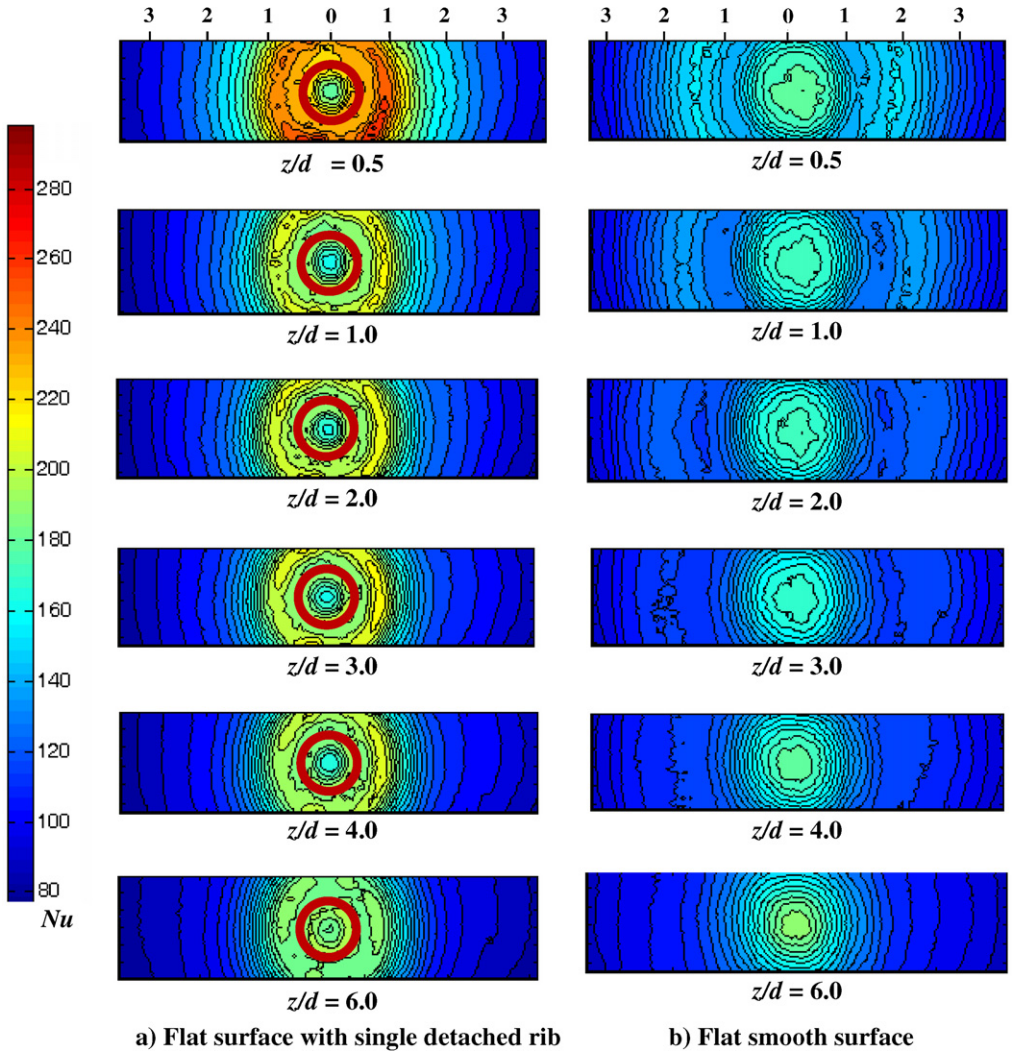

Fig. 10. Contour maps showing local distribution of heat transfer coefficients due to jet impingement on flat surface with and without single detached axisymmetric rib at $Re = 20{,}000$.

measured in terms of the respective rib heights from the sole rib at $r_1/d = 0.33$ are different i.e., peak locations of ribs of height $e/d = 0.13$, 0.23, 0.33 and 0.4, respectively, occur at $x/e = 2.8$, 2.2, 1.8 and 1.5, where x is the radial distance from the inner circumference of the single rib. It means, smaller the rib height farther is the peak location estimated in terms of the rib height. This may be attributed to flow velocities along the target surface decaying at a faster rate in the radial direction with increase in the rib height. Average heat transfer coefficients up to r/d of about 2.0 are higher for rib height of $e/d = 0.23$ for all z/d s except z/d of 0.5.

Thus, the detached rib configuration of single rib with $r_1/d = 0.33$, clearance under the rib (c/d) of 0.067, width of the rib (w/d) of 0.13 and height of the rib ($e/d = 0.23$) has better heat transfer distribution within a region of about $0 \leqslant r/d < 2.0$. Contour maps for the local distribution of Nusselt number due to jet impingement on a flat surface with single detached rib for different z/d are shown in Fig. 10a. Fig. 10b shows the corresponding contour maps for jet impingement on a smooth surface. The comparison of the two figures for a given z/d indicates that heat transfer coefficients around the stagnation point are higher with the ribbed

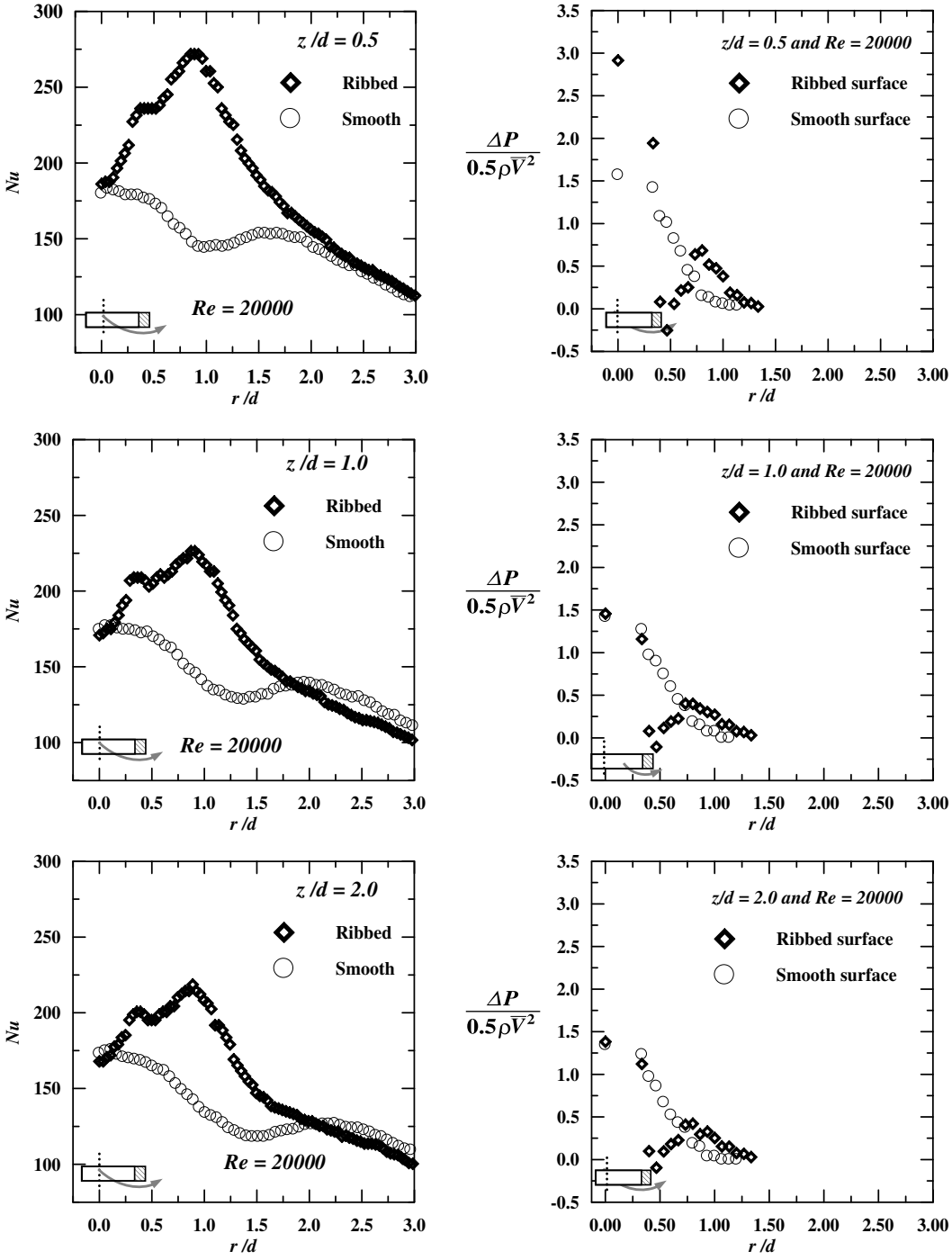

Fig. 11. Radial distribution of heat transfer coefficients and wall static pressure on the flat smooth surface and ribbed surface.

surface. It is observed in the stagnation region that Nusselt number increases from the stagnation point for the ribbed surface whereas it decreases for smooth surface. However, the Nusselt numbers at the stagnation point for both smooth and ribbed surfaces are comparable at any given z/d. Enhancements at $z/d = 0.5$ are higher. At larger jet-to-plate distances (z/d) augmentations decrease.

4.2. Radial distribution of wall static pressure over target plate

Wall static pressures over target plate are measured for surface with detached rib for the better configuration of heat transfer characteristics (single rib, $r_1/d = 0.33$, $c/d = 0.067$, $w/d = 0.13$ and $e/d = 0.23$). The values are compared with the corresponding case of smooth surface. Figs. 11 and 12 show the radial distribution of Nusselt number and non-dimensional wall static pressure for flat smooth surface and ribbed surface at Reynolds number of 20,000 and different jet-to-plate spacing. It is observed that wall static pressure gradient in the vicinity of stagnation point is higher for surface with detached ribs than flat smooth surface. These gradients decrease with higher z/d. For all z/d s, wall static pressure becomes sub-atmospheric under the rib and increases in the downstream upto an r/d of about 0.8. The wall static pressure de-

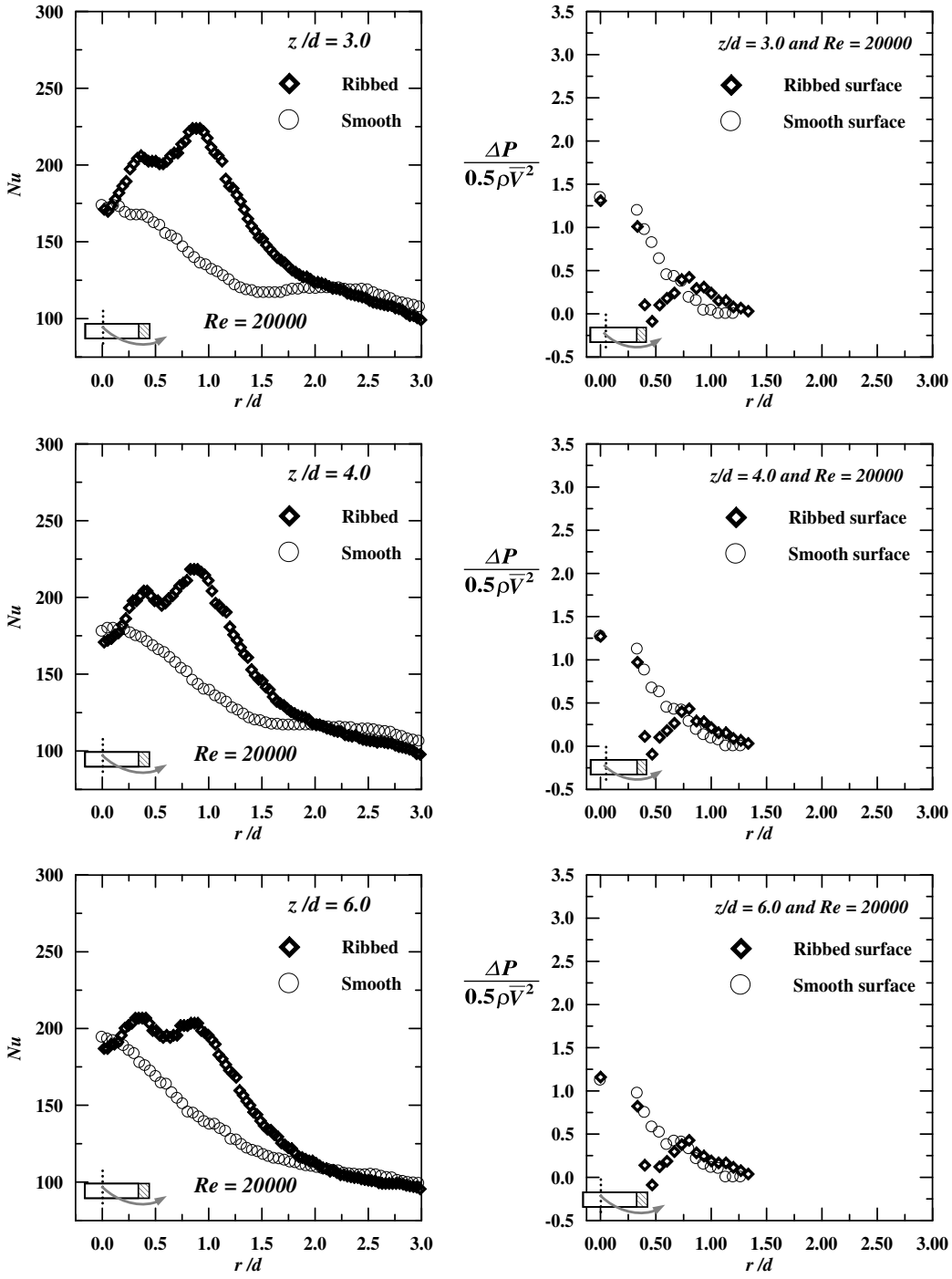

Fig. 12. Radial distribution of heat transfer coefficients and wall static pressure on the flat smooth surface and ribbed surface.

creases monotonically in the downstream until it is equal to the atmospheric pressure. Sharp decrease in pressure just ahead of the rib may create acceleration of the fluid in the upstream of the rib and hence local Nusselt numbers increase from stagnation point towards the rib. The location of second peak in the wall static pressure corresponds almost to the location of another peak in local Nusselt number. The second peak in the wall static pressure is higher for lower z/d. The heat transfer at the second peak also follows this trend.

4.3. Radial distribution of near-wall turbulent intensity and velocity

Near-wall turbulent intensity and velocity measurements are carried out over the surface with detached rib for the better configuration of heat transfer characteristics (single rib, $r_1/d = 0.33$, $c/d = 0.067$, $w/d = 0.13$ and $e/d = 0.23$) using hot-wire anemometer. The wire is oriented parallel to the target surface and perpendicular to radial wall-flow. The wire is located at $y/d = 0.067$ from the surface. The probe is traversed radially parallel to the target surface from $r/d = 0.5$–2.3 in steps of $r/d = 0.053$. Fig. 13a shows the radial distribution of near-wall turbulent intensities normalized with mean velocity at the nozzle exit $\left(100 \times \sqrt{\overline{u'^2}}/\overline{V}\right)$ on the flat surface with single detached rib at different jet-to-plate distances in the presence of normal jet impingement. Fig. 13b shows the corresponding radial distribution of near-wall velocities normalized with mean velocity. Fig. 13a indicates that the turbulent intensity increases sharply and peaks at an r/d of about 0.85. The value of peak turbulent intensity at $z/d = 0.5$ is about 17.5% and they decrease for higher jet-to-plate distance. At $z/d = 1.0$, 2.0 and 3.0, the values of peak turbulent intensity are nearly same and are about 15.2%. The corresponding values at $z/d = 4.0$ and 6.0 are about 14.3% and 13.7%, respectively. These observations show better matching with Nusselt number distribution in this region. Further the turbulent intensities decrease to a minimum. A secondary maximum in turbulent intensities are observed at higher radial locations. These minimum and maximum points shift away from the stagnation point with increase in jet-to-plate distances. Moreover, the values of turbulent intensities at the minimum and maximum decrease with increase in jet-to-plate distances. Fig. 13b shows that near-wall velocities increase in the radial direction from an $r/d = 0.5$ and reaches a point of maximum velocity. The values of the peak velocities are higher for lower z/d s. Further, the velocities decay monotonically. The radial location of maximum velocity shifts away from the stagnation point with increase in jet-to-plate distances. At $z/d = 1.0$, maximum near-wall velocity occurs at an r/d of about 1.0 where as this location shifts to about 1.4 for $z/d = 6.0$. Thus, the radial distribution of near-wall turbulent intensities shows better correlation with local heat transfer distribution.

4.4. Comparison of average heat transfer coefficients due to impinging jet on surface with detached rib and smooth surface

Sequential parametric heat transfer study of jet impingement on a flat surface with detached ribs show that a configuration of single detached rib at $r_1/d = 0.33$, rib height (e/d) of 0.23, rib width (w/d) of 0.13 and clearance under the rib (c/d) of 0.067 performs better. Experiments for this configuration are conducted for $z/d = 0.5$, 1.0, 2.0, 3.0, 4.0 and 6.0 and Reynolds number of 5000, 10,000, 15,000 and 20,000. Average Nusselt numbers of ribbed surface are estimated and normalized with average Nusselt number for corresponding smooth surface up to different radial locations of $r/d = 0.5$, 0.75, 1.0, 1.25, 1.5 and 2.0. Fig. 14 shows the comparison of average Nusselt number between smooth and ribbed surface due to jet impingement. It is observed from Fig. 14 that $(\overline{Nu_r}/\overline{Nu_s})$ increases with Reynolds number. Maximum enhancements in average heat transfer are observed for $(\overline{Nu_r}/\overline{Nu_s})$ averaged up to r/d of 1.25 and 1.5 at Reynolds number 20,000. For $z/d = 0.5$ and $Re = 20000$, enhancements are about 45% upto $r/d = 1.5$ and 36% upto $r/d = 2.0$. At the same Reynolds number and $z/d = 1.0$ and 2.0, enhancements are about 30% upto $r/d = 1.5$ and 25% upto $r/d = 2.0$. But a little higher enhancements are observed for $z/d = 3.0$. Enhancements decrease with higher z/d and for $z/d = 4.0$ and 6.0 corresponding augmentations are around 22%.

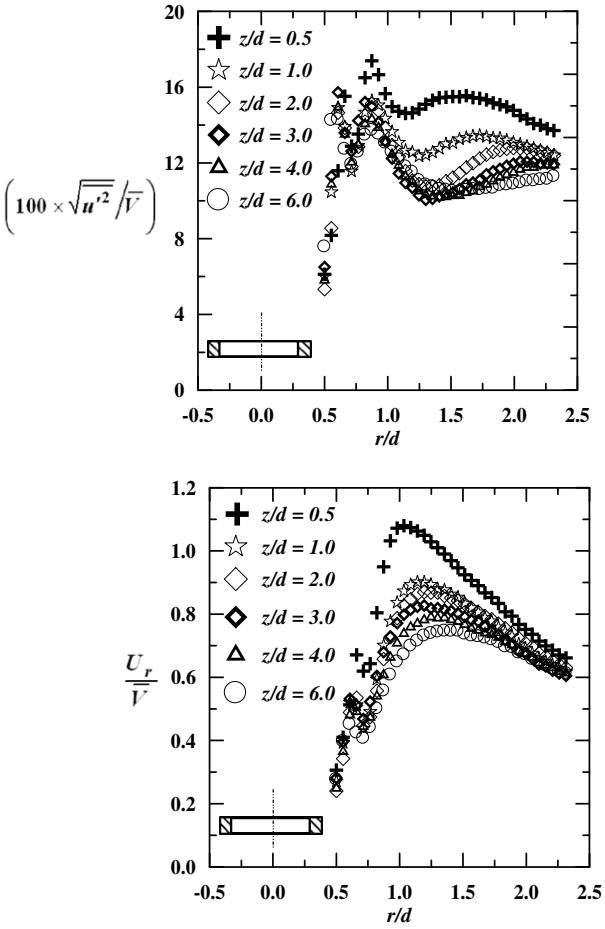

Fig. 13. Radial distribution of near-wall turbulent intensities and radial velocities on the flat surface with detached rib due to jet impingement.

Correlation is developed for Nusselt number averaged upto $r/d = 1.5$ and is expressed as in

$$\overline{Nu_r} = 0.33 Re^{0.65} (z/d)^{-0.08} \quad (7)$$

Values estimated from above correlation compare with the experimental values within ±6%.

5. Conclusions

An experimental study is carried out to investigate heat transfer enhancements between normally impinging circular air jet and a flat surface with axisymmetric detached rib-roughenes. A single jet from a long pipe nozzle which develops fully developed flow is chosen. Reynolds number based on nozzle exit condition is varied between 5000 and 20,000. Different configurations of detached ribs are arranged axisymmetrically on the target plate. Sequential parametric study is carried out to investigate the influence of different rib parameters on the local distribution of heat transfer coef-

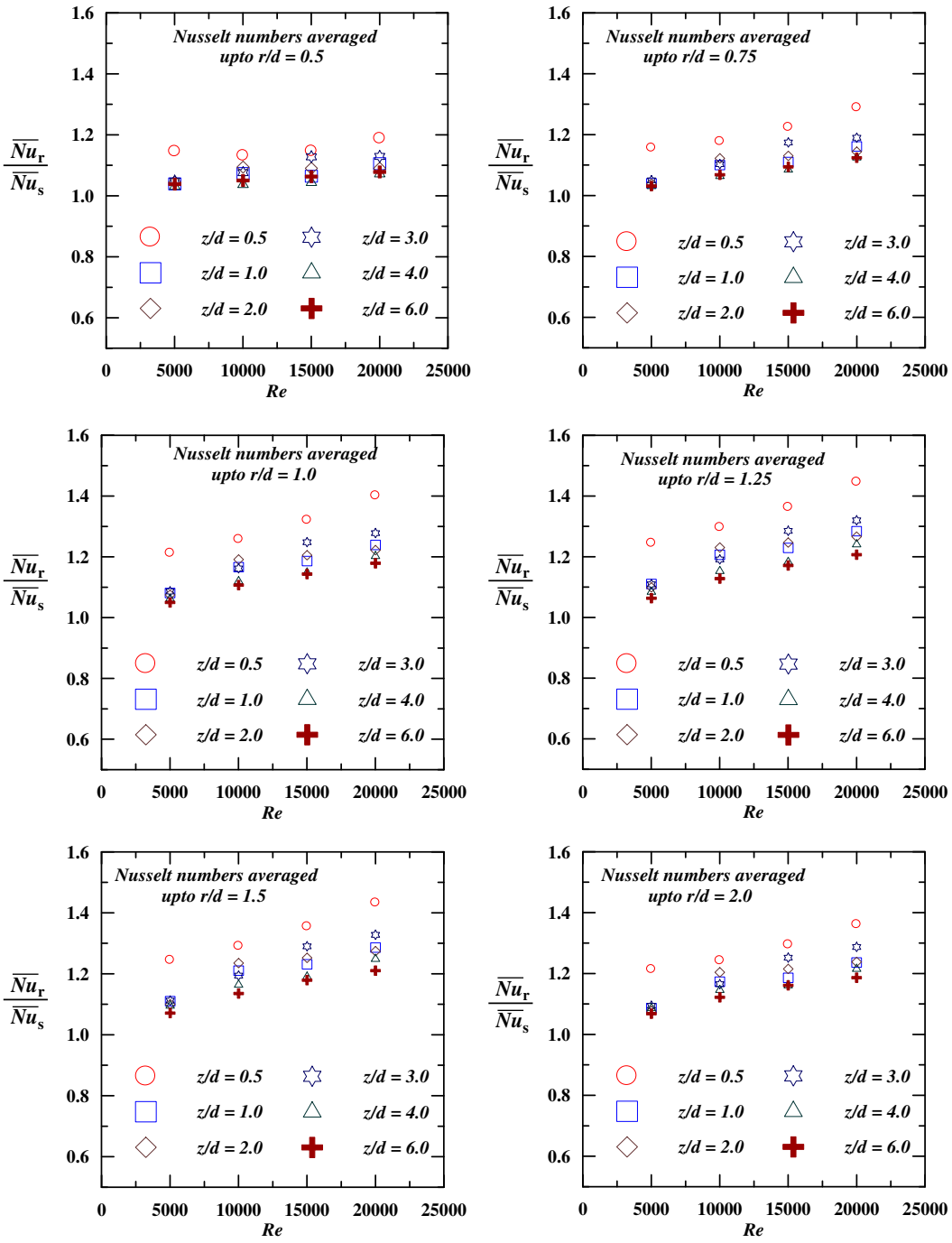

Fig. 14. Comparison of average Nusselt number to impinging air jet up to different radii between the detached ribs on flat surface and smooth surface.

ficients. The jet-to-plate distance is varied from 0.5 to 6 times the nozzle diameters. The results are compared with the radial heat transfer distribution between impinging jet and smooth surface. Near-wall turbulent intensity, velocity and wall static pressure measurements are made for the configuration identified as better one from heat transfer studies. The conclusions from this investigation are as follows:

- There is a continuous enhancement in Nusselt numbers from stagnation point till the first detached rib for all the ribbed configurations studied. This may be attributed to fluid accelerations created in the stagnation region by the clearance under the first rib. This result is supported by lower wall static pressure under the rib, compared with smooth surface.
- Nusselt numbers at the stagnation are highest for the configurations with the first rib located at $r_1/d = 0.33$ and clearance under rib (c/d) of 0.067. These values are comparable with that of smooth surface.
- Higher rib widths lead to drop in Nusselt numbers in the downstream of first rib and this may be due to major jet flow at its periphery miss to impact the target surface. But rib width (w/d) of 0.13 performed better and dropping trend behind the first rib almost disappeared.
- Second detached rib located closer to the first i.e., lower pitch between the ribs, retards the enhancements ahead of first rib and stagnation point Nusselt numbers drop as well. Single rib ($p/e = \infty$) located at $r_1/d = 0.33$ provides better radial distribution of Nusselt numbers than other configurations.

- For the best configuration investigated, it is seen that enhancements in the local Nusselt numbers at $Re = 20{,}000$ when compared with that of smooth surface case at around $r/d = 0.8$ are about 70–80% and highest for $z/d = 0.5$. This is because of higher near-wall turbulent intensity in this region.
- Increase in Reynolds number increases average Nusselt numbers averaged upto above $r/d = 0.75$ in comparison with a smooth surface case under same flow conditions. For $z/d = 0.5$ and $Re = 20000$, enhancements in average Nusselt numbers over smooth surface are about 45% enhancements decrease with higher z/d s.
- Correlation is developed for Nusselt number averaged upto $r/d = 1.5$ for the best configuration of detached-rib surface investigated.

References

Baughn, J.W., Shimizu, S., 1989. Heat transfer measurements from a surface with uniform heat flux and an impinging jet. J. Heat Transfer 111, 1096–1098.

Chakroun, W.M., Abdel-Rahman, A.A., Al-Fahed, S.F., 1998. Heat transfer augmentation for air jet impinged on a rough surface. Appl. Therm. Eng. 18, 1225–1241.

Ekkad, S.V., Kontrovitz, D., 2002. Jet impingement heat transfer on the dimpled target surfaces. Int. J. Heat Fluid Flow 23, 22–28.

Gao, N., Sun, H., Ewing, D., 2003. Heat transfer to impinging round jets with triangular tabs. Int. J. Heat Mass Transfer 46, 2557–2569.

Gardon, R., Akfirat, C., 1965. The role of turbulence in determining the heat transfer characteristics of impinging jet. Int. J. Heat Mass Transfer 8, 1261–1272.

Gardon, R., Akfirat, C., 1966. Heat transfer characteristics of impinging two dimensional air jets. J. Heat Transfer 88, 101–108.

Gardon, R., Cobonpue, J., 1962. Heat transfer between a flat plate and jets of air impinging on it. Int. Develop. Heat Transfer, ASME, 454–460.

Gau, C., Lee, C.C., 1992. Impingement cooling flow structure and heat transfer along rib-roughened walls. Int. J. Heat Mass Transfer 35, 3009–3020.

Gau, C., Lee, I.C., 2000. Flow and impingement cooling heat transfer along triangular rib-roughened walls. Int. J. Heat Mass Transfer 43, 4405–4418.

Hansen, L.G., Webb, B.W., 1993. Air jet impingement heat transfer from modified surfaces. Int. J. Heat Mass Transfer 36, 989–997.

Hrycak, P., 1983. Heat transfer from round impinging jets to a flat plate. Int. J. Heat Mass Transfer 26, 1857–1865.

Jambunathan, K., Lai, E., Moss, M.A., Button, B.L., 1992. A review of heat transfer data for single circular jet impingement. Int. J. Heat Fluid Flow 13, 106–115.

Katti, V.V., Prabhu, S.V., 2008. Experimental study and theoretical analysis of local heat transfer distribution between smooth flat surface and impinging air jet from a circular straight pipe nozzle. Int. J. Heat Mass Transfer. doi:10.1016/j.ijheatmasstransfer.2007.12.024.

Lee, D.H., Song, J., Jo, Myeong Chan, 2004. The effect of nozzle diameter on impinging jet heat transfer and fluid flow. J. Heat Transfer 126, 554–557.

Liou, T.M., Wang, W.B., 1995. Laser holographic interferometry study of developing heat transfer in a duct with a detached rib array. Int. J. Heat Mass Transfer 38, 91–100.

Liou, T.M., Wang, W.B., Chang, Y.-J., 1995. Holographic interferometry study of spatially periodic heat transfer in a channel with ribs detached from one wall. J. Heat Transfer 117, 32–39.

Liou, T.M., Yang, C.-P., Lee, H.-L., 1997. LDV measurements of spatially periodic flows over a detached solid-rib array. J. Fluid. Eng. 119, 383–389.

Liou, T.M., Shuy, W.J., Tsao, Y.H., 1998. Effect of rib height and pitch on the thermal performance of a passage disturbed by detached solid ribs. J. Turbomach. 12, 581–588.

Livingood, J.N.B., Hrycak, P., 1970. Impingement heat transfer from turbulent air jets to flat plates – a literature survey. NASA Technical Memorandum (NASA TM X-2778).

Lytle, D., Webb, B.W., 1994. Air jet impingement heat transfer at low nozzle plate spacings. Int. J. Heat Mass Transfer 37, 1687–1697.

Martin, H., 1977. Heat and mass transfer between impinging gas jets and solid surface. Adv. Heat Transfer 13, 1–60.

Miyake, G., Hirata, M., Kasagi, N., 1994. Heat transfer characteristics of an axisymmetric jet impinging on a wall with concentric roughness elements. Exp. Heat Transfer 7, 121–141.

Moffat, R.J., 1988. Describing the uncertainties in experimental results. Exp. Therm. Fluid Sci. 1, 3–17.

Tsia, J.P., Hwang, J.J., 1999. Measurements of heat transfer and fluid flow in a rectangular duct with alternate attached–detached rib array. Int. J. Heat Mass Transfer 42, 2071–2083.

Viskanta, R., 1993. Heat transfer to impinging isothermal gas and flame jets. Exp. Therm. Fluid Sci. 6, 111–134.